

Standard Model measurements with ATLAS

Mateusz Dyndal¹ on behalf of the ATLAS Collaboration
AGH University of Science and Technology
al. Mickiewicza 30, 30-059 Krakow, Poland

A broad range of Standard Model measurements performed in proton–proton collisions with the ATLAS detector at the LHC is reviewed. The latest results are obtained at the center-of-mass energy of both 7 TeV and 8 TeV, which cover total cross sections, fiducial cross sections, differential cross sections (if available) and comparison with theory predictions. These measurements provide important tests for QCD and electroweak interactions, Electroweak Symmetry Breaking over a broad kinematic range. Searches for new physics are also performed by probing anomalous gauge bosons couplings.

1 Introduction

The ATLAS experiment [1] is one of the four large experiments at the Large Hadron Collider (LHC). The ATLAS detector is a general purpose particle physics detector with forward-backward symmetric cylindrical geometry. During the year 2011, ATLAS recorded proton–proton (pp) collision data corresponding to an integrated luminosity of 4.6 fb^{-1} at the center-of-mass energy of 7 TeV. In 2012, 20.7 fb^{-1} of pp data were recorded at the center-of-mass energy of 8 TeV, which is summarized in Fig. 1. Using all of this data, ATLAS has performed a wide range of Standard Model physics analyses, where some of which are reviewed in these proceedings.

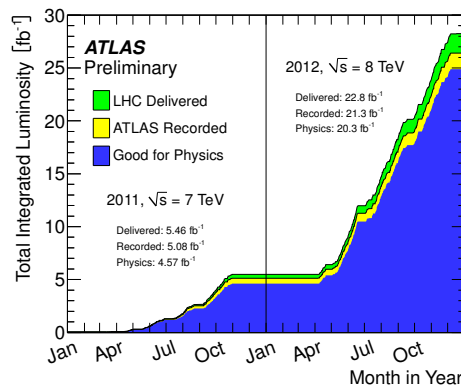


Figure 1: Cumulative luminosity versus time for ATLAS during stable LHC beams in pp collisions at 7 TeV and 8 TeV center-of-mass energies in 2011 and 2012. The overlaid histograms in top-to-bottom order show the amount of data delivered to, recorded by ATLAS, and certified to be good quality [2].

¹Mateusz.Dyndal@cern.ch

The ATLAS Standard Model physics results can be divided into four main categories: soft QCD, diffraction and forward physics; electroweak physics (including W/Z bosons and multi-bosons measurements); jet physics and direct photons physics. In each of the sub-fields, only a few recent results are detailed. All ATLAS Standard Model results can be found at the ATLAS Standard Model public results webpage [3].

2 Soft QCD, diffraction and forward physics

The following three major topics of soft QCD, diffractive and forward physics domain are highlighted following up the latest publications of ATLAS: total pp cross section at 7 TeV with ALFA, the exclusive dilepton production cross section and the underlying event in Z -boson production.

2.1 Total pp cross section at 7 TeV with ALFA

The total pp cross section is a fundamental parameter of strong interactions. In ATLAS, a measurement of the total cross section has been made from elastic pp scattering in special runs with high- β^* beam optics, with an integrated luminosity of $80 \mu\text{b}^{-1}$ and protons detected by the ALFA detector [4]. This detector is housed in the 4 roman pots at ± 238 m and ± 241 m from the ATLAS interaction point and is designed to detect small-angle proton scattering.

The elastic cross section can be calculated through the following equation:

$$\frac{d\sigma_{\text{el}}}{dt} = \frac{1}{16\pi} \left| f_{\text{N}}(t) + f_{\text{C}}(t)e^{i\alpha\phi(t)} \right|^2, \quad (1)$$

where $f_{\text{N}}(t)$ is the strong interaction amplitude, $f_{\text{C}}(t)$ is the Coulomb amplitude, $\phi(t)$ is a phase induced by long-range Coulomb interactions and $-t = (\theta^* \times p)^2$ is the four-momentum transfer (where p is the nominal proton beam momentum and θ^* is the scattering angle at interaction point that is measured from the proton scattering trajectory in ALFA).

The function $f_{\text{N}}(t)$ can be written using exponential relation, $e^{-Bt/2}$, where B is the nuclear slope parameter. At sufficiently low $-t$, $f_{\text{N}}(t)$ is dominant with respect to the $f_{\text{C}}(t)$ parameter and the elastic cross section becomes a function only of a single exponential form. Therefore, for the fit of the elastic cross section, protons in the range $0.01 \text{ GeV}^2 < -t < 0.1 \text{ GeV}^2$ have been selected in ALFA, giving the value:

$$B = 19.73 \pm 0.14(\text{stat.}) \pm 0.26(\text{syst.}) \text{ GeV}^{-2}.$$

The total cross section is obtained through the optical theorem:

$$\sigma_{\text{tot}}^2 = \frac{16\pi}{1 + \rho^2} \frac{d\sigma_{\text{el}}}{dt} \Big|_{t \rightarrow 0}, \quad (2)$$

where ρ is a small correction arising from the ratio of the real-to-imaginary part of the elastic scattering amplitude and is taken from the theory. It is measured to be:

$$\sigma_{\text{tot}} = 95.4 \pm 1.3(\text{tot.}) \text{ mb}.$$

The results on the total and elastic cross sections are in agreement with the previous experiments, as shown in Fig. 2.

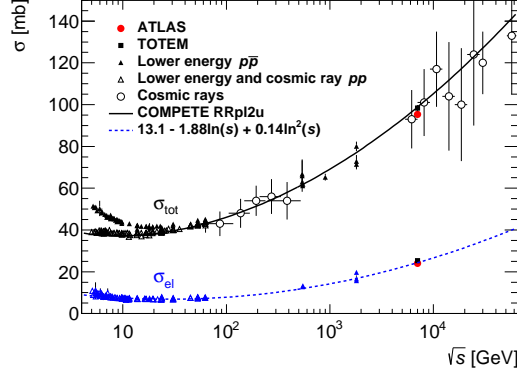


Figure 2: Total and elastic pp cross sections as function of the pp center-of-mass energy. ATLAS results (full circles) are compared with previous results [4].

2.2 Exclusive $\gamma\gamma \rightarrow \ell^+\ell^-$ production in pp collisions at 7 TeV

Two-photon interactions make an important class of processes at the LHC. A measurement of the exclusive cross section for the reaction $\gamma\gamma \rightarrow \ell^+\ell^-$ ($\ell = e, \mu$) in pp collisions at center-of-mass energy of $\sqrt{s} = 7$ is performed with the ATLAS experiment [5]. Using 4.6 fb^{-1} of data, the fiducial cross sections for exclusive two-photon production of lepton pairs are measured using events passing exclusive selection with the veto on additional charged-particle track activity (Fig. 3a). Signal is extracted by fitting the dilepton acoplanarity distributions to data, which is demonstrated in Fig. 3b.

The resulting cross section for the electron channel is measured to be:

$$\sigma_{\gamma\gamma \rightarrow e^+e^-}^{\text{excl.}} = 0.428 \pm 0.035(\text{stat.}) \pm 0.018(\text{syst.}) \text{ pb} ,$$

for the kinematical domain $m_{e^+e^-} > 24 \text{ GeV}$, $p_T^e > 12 \text{ GeV}$ and $|\eta^e| < 2.4$. This value can be compared with the theoretical predictions, including absorptive corrections to account for the finite size of the proton:

$$\sigma_{\gamma\gamma \rightarrow e^+e^-}^{\text{EPA, corr.}} = 0.398 \pm 0.007(\text{theo.}) \text{ pb} .$$

For the muon channel, the cross section is measured to be

$$\sigma_{\gamma\gamma \rightarrow \mu^+\mu^-}^{\text{excl.}} = 0.628 \pm 0.032(\text{stat.}) \pm 0.021(\text{syst.}) \text{ pb} ,$$

for $m_{\mu^+\mu^-} > 20 \text{ GeV}$, $p_T^\mu > 10 \text{ GeV}$, $|\eta^\mu| < 2.4$. This measured value can be also compared with the theory:

$$\sigma_{\gamma\gamma \rightarrow \mu^+\mu^-}^{\text{EPA, corr.}} = 0.638 \pm 0.011(\text{theo.}) \text{ pb} .$$

With its improved statistical precision compared to the previous measurements, this analysis provides a better understanding of the physics of two-photon interactions at hadron colliders.

2.3 Underlying event in inclusive Z -boson production

Underlying event (UE) activity at hadron colliders includes partons not participating in the hard-scattering process (beam remnants), and additional hard scatters in the same pp collision, termed multiple parton interactions (MPI). Initial and final state gluon radiation (ISR, FSR) also contribute to the UE activity.

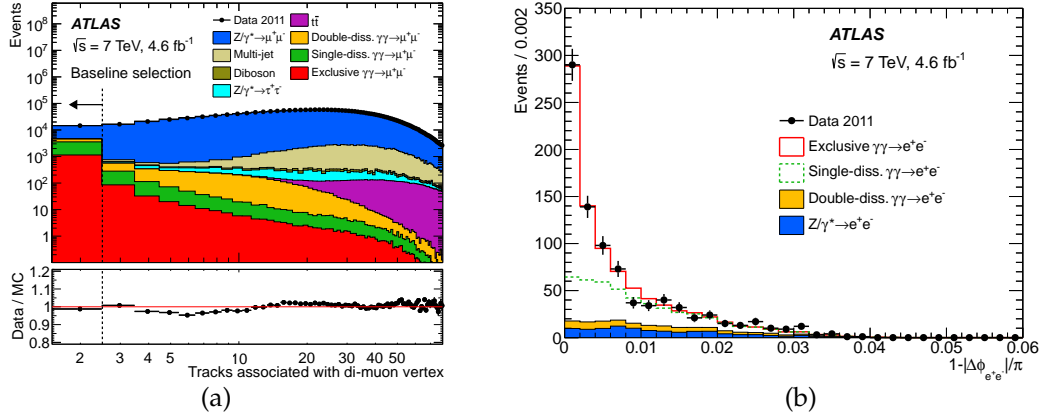


Figure 3: (a) Number of tracks associated with the dimuon vertex. (b) Dielectron acoplanarity distributions for the selected sample after exclusivity requirements. Data are shown as points with statistical error bars, while the stacked histograms represent the expected signal and background levels [5].

In this analysis [6] events with a Z-boson candidate decaying into an electron or muon pair are selected. The azimuthal space around the Z-boson direction is taken into account by dividing it in 4 sub-regions: the "toward", closest to the Z-boson direction ($|\Delta\phi| < 60^\circ$, where $\Delta\phi = 0^\circ$ denotes the Z-boson direction), the "away", opposite to the Z-boson direction ($|\Delta\phi| > 120^\circ$) and two transverse regions ($60^\circ < |\Delta\phi| < 120^\circ$). Transverse and toward regions are the most sensitive to the UE activity.

The UE activity is studied in terms of normalized and differential distributions using charged-particle tracks with $p_T > 0.5$ GeV and $|\eta| < 2.5$. The results are compared with a variety of Monte Carlo generators (see Fig. 4a). Finally, a comparison with other experiments with a jet (instead of a Z-boson) as a hard-scattering object has been made. Fig. 4b shows that at high- p_T the charged-particle density profile can be treated as a very universal quantity.

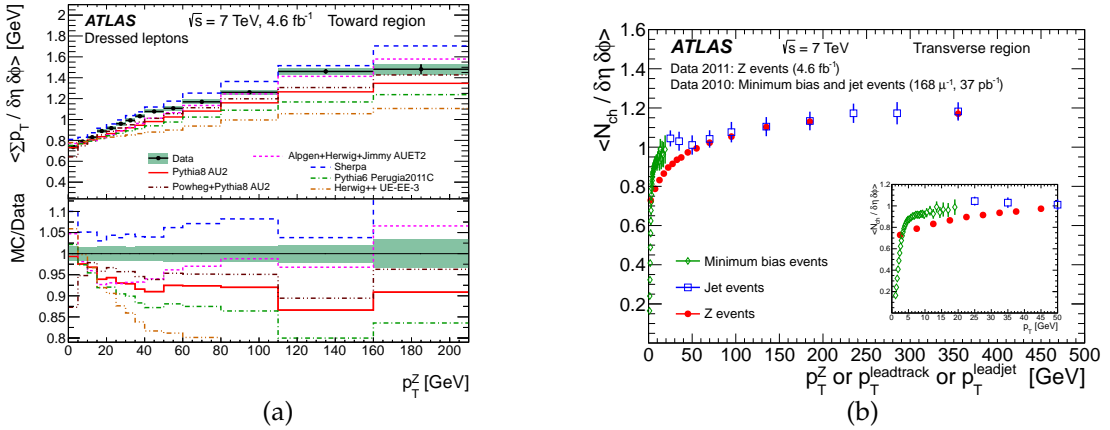


Figure 4: (a) Comparison of data and Monte Carlo predictions for charged particle scalar Σp_T density profile, as a function of Z-boson transverse momentum. (b) Charged-particle multiplicity profile compared between different hard-scattering object as function of its transverse momentum [6].

3 Electroweak physics (W/Z bosons)

The latest ATLAS measurements of vector boson (W/Z) production properties involve the following physics results: the W +jets differential cross section, the low-mass Drell–Yan (Z/γ^*) differential cross-section and the forward-backward asymmetry of the Z boson.

3.1 W +jets cross section at 7 TeV

The W +jets differential cross section is measured using fully leptonic decay final states of the W boson (e^\pm or μ^\pm) [7]. Jets are reconstructed using the anti- k_t algorithm with a radius parameter $R = 0.4$ and are required to have $p_T^j > 30$ GeV and rapidity of $|y_j| < 4.4$.

The 4.6 fb^{-1} of 7 TeV collision data allow for a precise measurement of the W +jets cross section (for the first time) up to seven jets. This is presented in Fig. 5. In the measurement, a large kinematic range is explored, including jet production up to a transverse momentum of 1 TeV.

The measurements are compared to numerous QCD predictions including next-to-leading-order perturbative calculations, resummation calculations and Monte Carlo generators. Fixed-order predictions provide overall a good description of the data, but have greater difficulty describing some jet-related variables in kinematic regions where the dominant production mechanism is dijet production, followed by the emission of a W boson from one of the quarks.

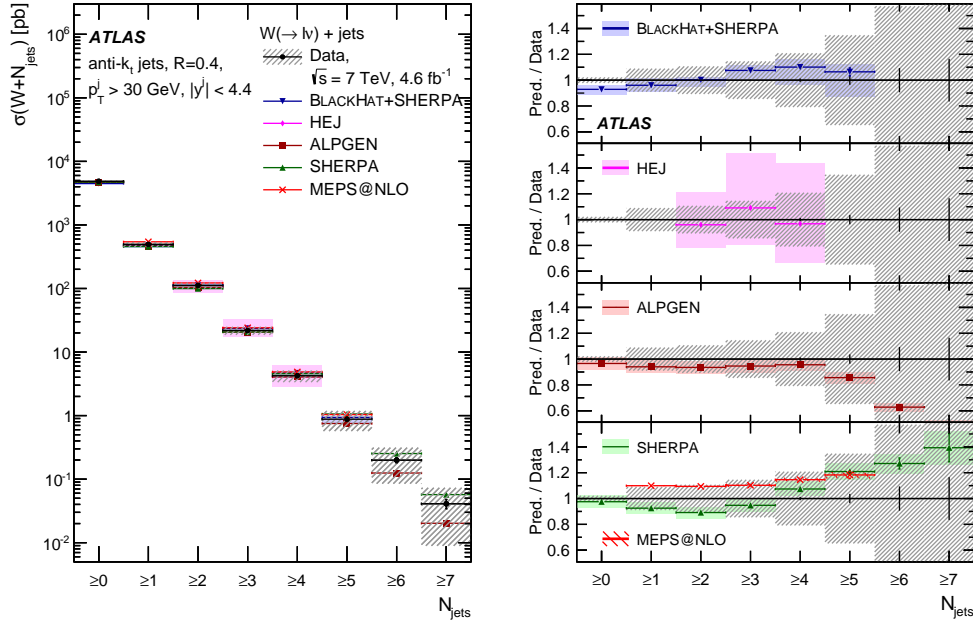


Figure 5: Cross section for the production of W +jets as a function of the inclusive jet multiplicity, compared to the predictions from various models. The left-hand plot shows the differential cross sections and the right-hand plot shows the ratios of the predictions to the data [7].

3.2 Low-mass Drell–Yan differential cross section at 7 TeV

A single-differential Drell–Yan cross section (in the e^+e^- or $\mu^+\mu^-$ decay channels) as a function of $m_{\ell^+\ell^-}$ is measured by ATLAS in the range $12 \text{ GeV} < m_{\ell^+\ell^-} < 66 \text{ GeV}$ [8]. Such a low-mass production region is dominated by the electromagnetic coupling of the virtual photon (γ^*) to the quark-antiquark pair. This region exhibits different sensitivity to u and d -type quarks than the Z -pole region.

The measurement also includes the 2010 data set in which the transverse momentum thresholds for leptons were as low as 6 GeV and 9 GeV. The results are compared to various fixed-order calculations and different parton distribution functions (PDFs), as presented in Fig. 6. The calculations are also corrected for additional higher-order electroweak radiative effects, including a photon-induced contribution. In the lowest mass range, the measurement agrees better with the prediction from next-to-next-to-leading-order perturbative QCD calculation than that from next-to-leading-order.

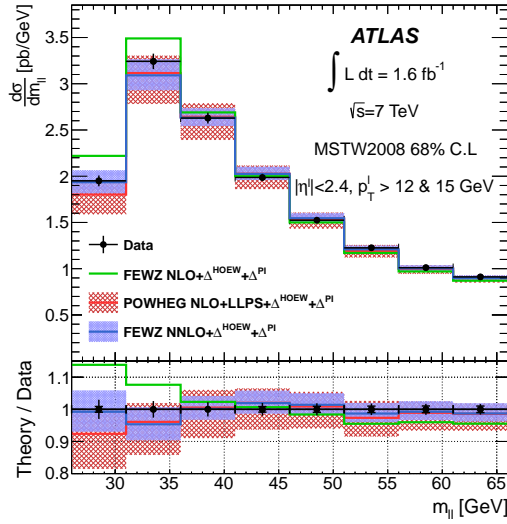


Figure 6: The measured fiducial differential cross section as a function of the dilepton invariant mass compared to various theory predictions. The data (solid points) are displayed at unity with the statistical (inner) and total (outer) measurement uncertainties [8].

3.3 Forward-backward asymmetry of the Z boson at 7 TeV

The electroweak theory predicts an asymmetry in the direction of the leptons produced in the $q\bar{q} \rightarrow Z \rightarrow \ell^+\ell^-$ reactions, with respect to the direction of the incoming quarks, in the rest frame of the dilepton system. Indeed the presence of both vector and axial-vector couplings of the Z boson to fermions leads to the non-zero asymmetry parameter:

$$A_{\text{FB}} = \frac{N_{\cos\theta_{\text{CS}}^* \geq 0}^{\text{ev}} - N_{\cos\theta_{\text{CS}}^* < 0}^{\text{ev}}}{N_{\cos\theta_{\text{CS}}^* \geq 0}^{\text{ev}} + N_{\cos\theta_{\text{CS}}^* < 0}^{\text{ev}}}, \quad (3)$$

defined using the angle between the negatively-charged lepton relative to the incoming quark direction, θ_{CS}^* .

ATLAS has measured this asymmetry using $Z \rightarrow e^+e^-$ or $Z \rightarrow \mu^+\mu^-$ events [9]. As shown in Fig. 7a, the measured asymmetry distributions are found to be consistent with theoretical predictions in the whole mass region. The effective weak mixing angle, $\sin^2 \theta_{\text{eff}}^{\text{lept}}$, is also extracted and compared with the previous measurements (Fig. 7b). The combination of the two decay channel yields a value of:

$$\sin^2 \theta_{\text{eff}}^{\text{lept}} = 0.2308 \pm 0.0012(\text{tot.}) .$$

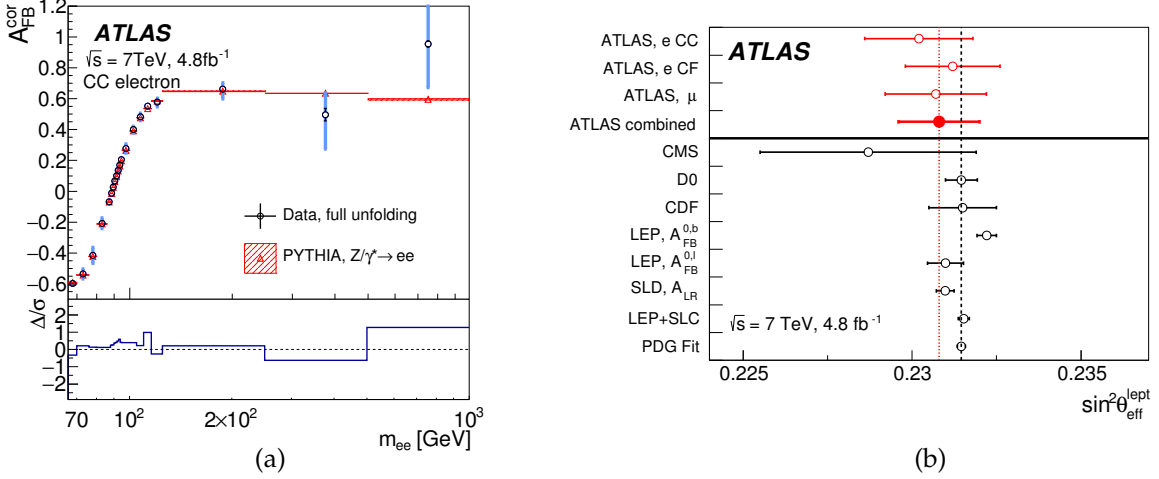


Figure 7: (a) Forward-backward asymmetry parameter values as a function of the dilepton invariant mass for the electron channel. (b) Comparison of the results of this analysis with other published results for $\sin^2 \theta_{\text{eff}}^{\text{lept}}$ [9].

4 Electroweak physics (multi-bosons)

The measurements of electroweak multi-boson production provide very important tests of the Standard Model. Such events are significant and irreducible backgrounds for the Higgs boson or Beyond Standard Model searches. The latest ATLAS results cover the $WW/WZ \rightarrow \ell\nu jj$ cross section measurement, the evidence of $W\gamma\gamma$ production and the electroweak production of $W^\pm W^\pm jj$.

4.1 $WW/WZ \rightarrow \ell\nu jj$ cross section measurement at 7 TeV

The combined production cross section of $WW + WZ$ is measured in semileptonic final states with one of the W/Z decaying into hadrons using 4.6fb^{-1} of 7 TeV data [10]. The cross section is extracted using a maximum-likelihood fit to the dijet invariant mass spectrum (demonstrated in Fig. 8a).

The fiducial cross section is measured to be:

$$68 \pm 7(\text{stat.}) \pm 19(\text{syst.}) \text{ pb}$$

and is consistent with the next-to-leading-order perturbative QCD prediction:

$$61.1 \pm 2.2(\text{theo.}) \text{ pb} .$$

The dijet transverse momentum distribution is used to set limits on anomalous triple gauge coupling vertices. This is presented in Fig. 8b. The limits on anomalous couplings are similar to those obtained by other analyses with diboson final states.

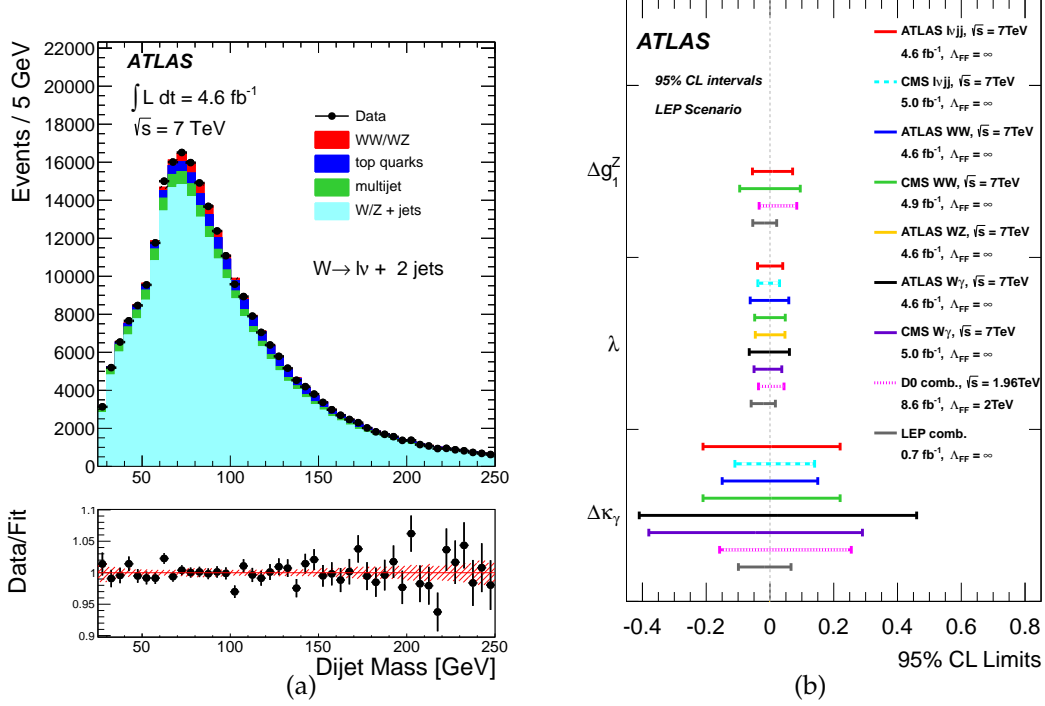


Figure 8: (a) Distributions of the dijet invariant mass for the sum of the electron and muon channels after the likelihood fit. (b) Comparison of limits on anomalous triple gauge coupling parameters obtained in this analysis with limits quoted by other experiments [10].

4.2 $W\gamma\gamma$ production at 8 TeV

The measurement of triboson production at 8 TeV in ATLAS is performed with 20.3 fb^{-1} of data in fully leptonic final states of W production and with two isolated photons [11]. Leptons (electrons or muons) and photons are required to have $p_T > 20 \text{ GeV}$. Fiducial cross sections are measured in both inclusive and exclusive additional-jet multiplicity channels:

$$\begin{aligned}\sigma_{N_j \geq 0} &= 6.1 \pm 1.1(\text{stat.}) \pm 1.2(\text{syst.}) \pm 0.2(\text{lumi.}) \text{ fb} , \\ \sigma_{N_j = 0} &= 2.9 \pm 0.8(\text{stat.}) \pm 1.0(\text{syst.}) \pm 0.1(\text{lumi.}) \text{ fb} .\end{aligned}$$

In comparison with the next-to-leading-order perturbative QCD calculation:

$$\begin{aligned}\sigma_{N_j \geq 0} &= 2.90 \pm 0.16(\text{theo.}) \text{ fb} , \\ \sigma_{N_j = 0} &= 1.88 \pm 0.20(\text{theo.}) \text{ fb} ,\end{aligned}$$

the exclusive jet channel shows good agreement, while inclusive cross section is higher by 1.9 standard deviations.

The exclusive jet channel with a further cut on diphoton invariant mass ($m_{\gamma\gamma} > 300$ GeV) is used for the anomalous quartic gauge coupling limit setting. The limits together with the $m_{\gamma\gamma}$ spectrum are shown in Fig. 9.

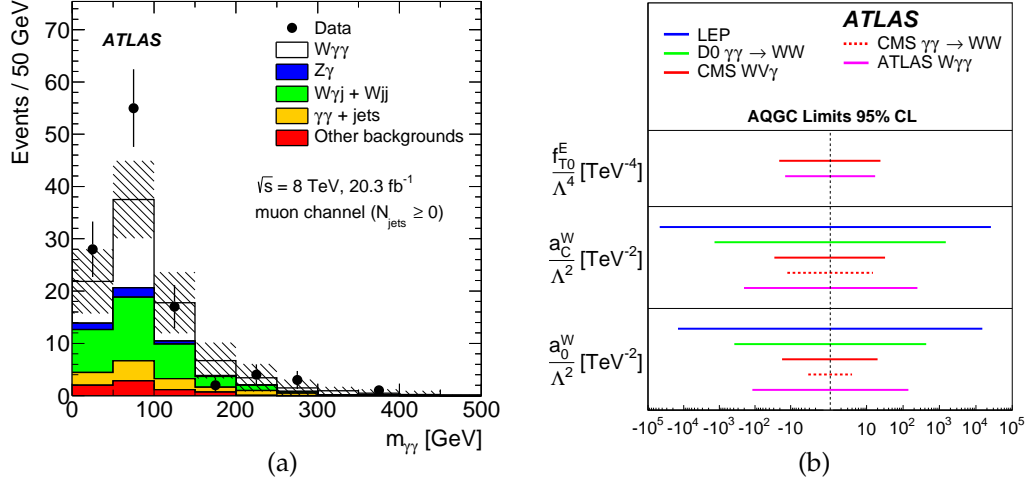


Figure 9: (a) The diphoton invariant mass distribution in data compared with predicted signal and estimated backgrounds in the muon channel for inclusive jet selection. (b) Anomalous quartic gauge coupling limits obtained using the measured high-mass region and exclusive jet selection, compared with limits from other experiments [11].

4.3 Electroweak $W^\pm W^\pm jj$ production at 8 TeV

The evidence of same-electric-charge vector boson scattering production at 8 TeV is observed for the first time [12]. Fully leptonic final states of W production and jets with $p_T^j > 30$ GeV, $|\eta_j| < 4.5$ are measured with 20.3 fb^{-1} of data.

The signal is extracted in a so-called vector boson scattering region that requires dijet invariant mass larger than 500 GeV and jets separated in rapidity by $|\Delta y_{jj}| > 2.4$. This selection is shown in Fig. 10. The fiducial cross section in this region is measured to be:

$$\sigma_{\text{VBS}} = 1.4 \pm 0.3(\text{stat.}) \pm 0.2(\text{syst.}) \text{ fb} ,$$

in agreement with the Standard Model expectations of:

$$\sigma_{\text{VBS}} = 0.95 \pm 0.06(\text{theo.}) \text{ fb} .$$

In addition, the first limits on the α_4, α_5 anomalous quartic gauge coupling parameters are set, as presented in Fig. 11.

5 Jet physics

Since the QCD processes at the LHC are the most abundant ones, a very good understanding of them is necessary. From the events with jets, perturbative and non-perturbative QCD can be tested. The latest ATLAS jet results cover the inclusive jet and three-jet differential cross section measurements.

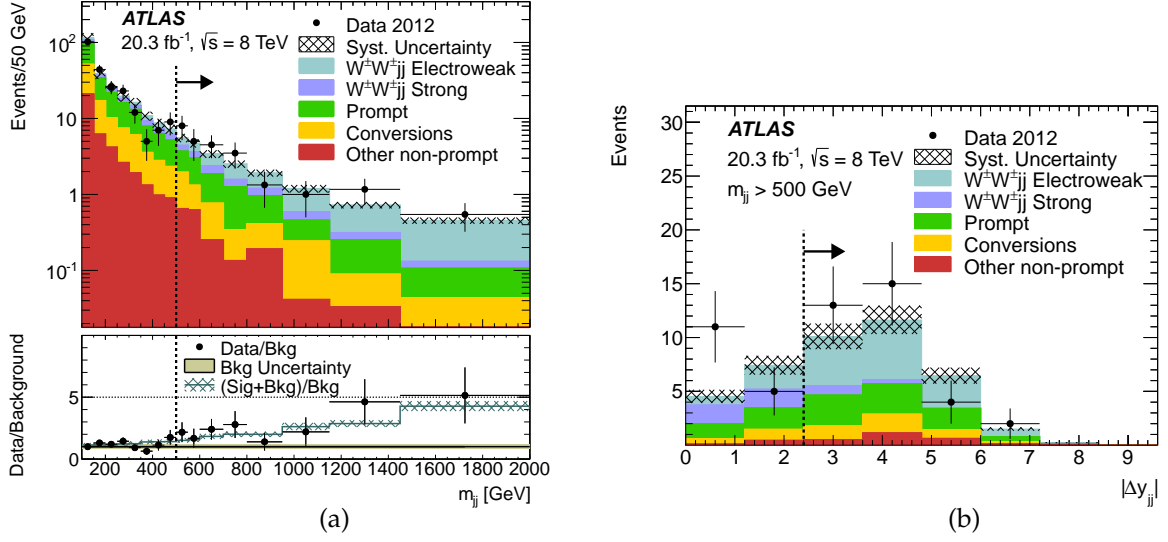


Figure 10: (a) The m_{jj} distribution for events passing the inclusive region selections except for the m_{jj} selection indicated by the dashed line. (b) The Δy_{jj} distribution for events passing all inclusive region selections [12].

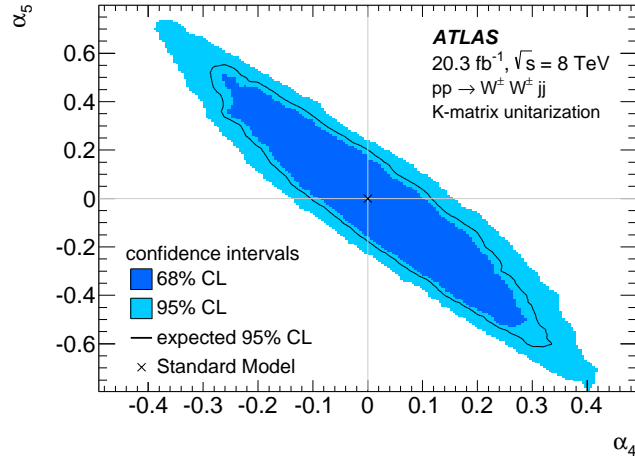


Figure 11: Limits on α_4, α_5 parameters. Points outside of the solid light ellipse are excluded by the data at 95% confidence level. Points outside the inner dark ellipse are excluded at the 68% confidence level. The expected exclusion is given by the solid line [12].

5.1 Inclusive jet cross section at 7 TeV

The double-differential inclusive jet cross sections for $\sqrt{s} = 7$ TeV is measured by ATLAS over jet transverse momenta from 100 GeV to 2 TeV in the rapidity region $|y_j| < 3$ [13]. Jets reconstructed with the anti- k_t algorithm and radius of both 0.4 and 0.6 are considered.

The next-to-leading-order perturbative QCD predictions calculated with corrections for non-perturbative and electroweak effects are compared to the measurement in Fig. 12a. This figure shows that the predictions reproduce the measured cross sections, which range over eight orders of magnitude in the jet rapidity bins. More detailed comparisons that include different proton PDF sets are shown in Fig. 12b.

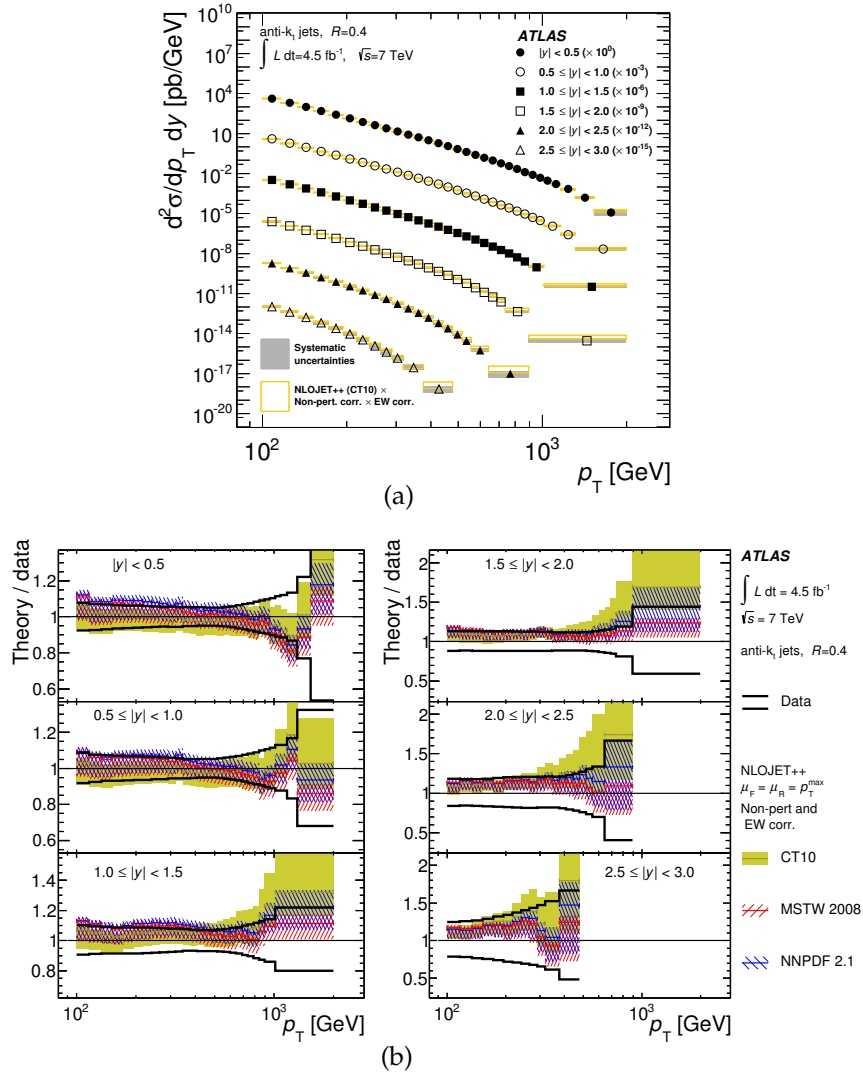


Figure 12: (a) Double-differential inclusive jet cross sections as a function of the jet p_T in bins of rapidity, for anti- k_t jets with $R = 0.4$. (b) Ratio of theory predictions to the measured double-differential inclusive jet cross sections for different proton PDF sets [13].

5.2 Three-jet production cross section at 7 TeV

A double-differential three-jet production cross section is measured as a function of the three-jet invariant mass and the sum of absolute rapidity separation between the three jets, $|Y^*| = |y_{j1} - y_{j2}| + |y_{j2} - y_{j3}| + |y_{j1} - y_{j3}|$ [14]. Jets with $p_T^{j1} > 150$ GeV, $p_T^{j2} > 100$ GeV and $p_T^{j3} > 50$ GeV are considered. The measurement is performed using the anti- k_t algorithm and two different values of the jet radius parameter, $R = 0.4$ and $R = 0.6$.

Figure 14 shows the comparison of the three-jet double-differential cross section as a function of m_{jjj} , binned in $|Y^*|$, to next-to-leading-order perturbative QCD predictions corrected for non-perturbative effects. The three-jet cross sections are measured for the first time up to $m_{jjj} = 5$ TeV which are well described by the predictions that also include different proton PDF sets.

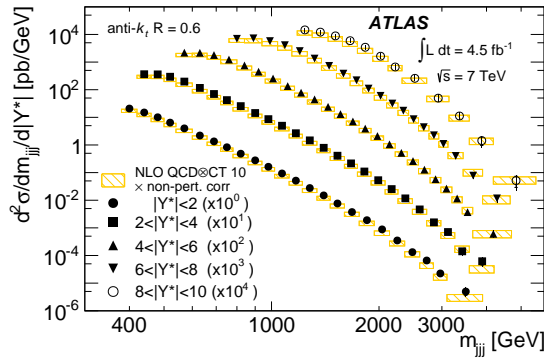


Figure 13: Three-jet double-differential cross section as a function of m_{jjj} in bins of $|Y^*|$. The jets are identified using the anti- k_t algorithm with $R = 0.6$ [12].

6 Direct photons physics

A measurement of isolated prompt photon production cross section provides an important test of perturbative QCD, with the possibility of using such a measurement to constrain the gluon PDFs.

The differential cross sections of Standard Model inclusive isolated prompt photon are measured in ATLAS as a function of photon E_T in the range $100 \text{ GeV} < E_T^\gamma < 1000 \text{ GeV}$ and two photon pseudorapidity ranges: barrel ($|\eta_\gamma| < 1.37$) and endcap ($1.52 < |\eta_\gamma| < 2.37$) [15]. The measurement agrees with the next-to-leading-order perturbative QCD prediction up to $E_T^\gamma = 1 \text{ TeV}$, which is presented in Fig. 14.

7 Summary and Outlook

The LHC Run-I has been very fruitful for the ATLAS collaboration, with both LHC machine and detector performance, high efficiencies of data taking and physics analyses. ATLAS performed a broad range of Standard Model physics measurements covering a variety of topics. Most of the measurements are published based on the full pp collisions dataset at 7/8 TeV. In general, the measured cross sections and parameters agree well with Standard Model predictions.

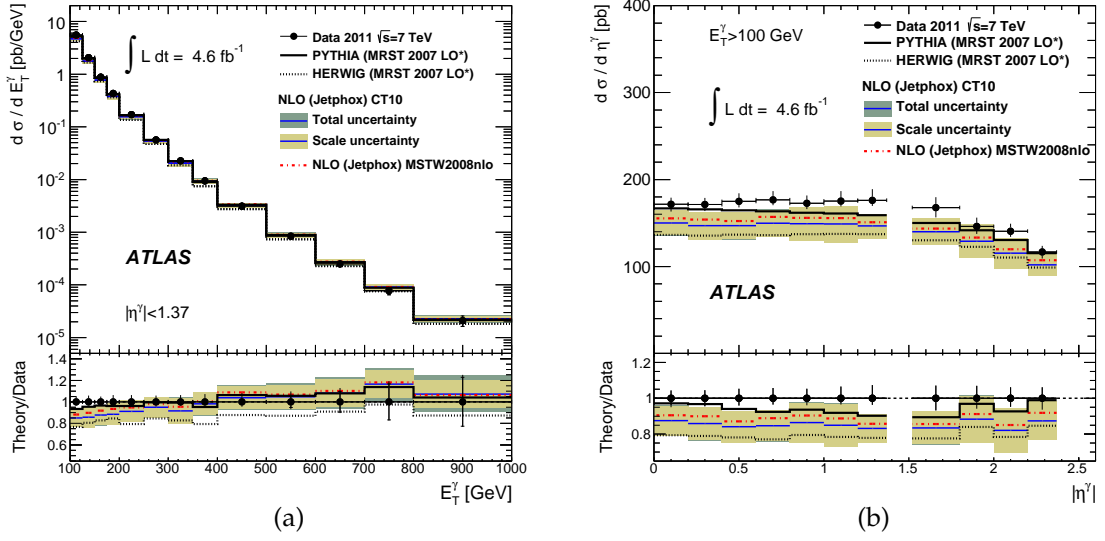


Figure 14: (a) Measured and expected inclusive prompt photon cross section as a function of the photon E_T in the barrel pseudorapidity region. (b) Measured and expected inclusive prompt photon cross section as a function of pseudorapidity for photons with $E_T > 100 \text{ GeV}$ [15].

A summary of the ATLAS Standard Model cross section measurements is shown in Fig. 15. The Standard Model measurements will continue in the forthcoming LHC runs at the new center-of-mass energy of 13 TeV.

Acknowledgments

This work was partly supported by the Polish National Science Centre under contract No. UMO-2012/05/B/ST2/02480 and by PL-Grid Infrastructure.

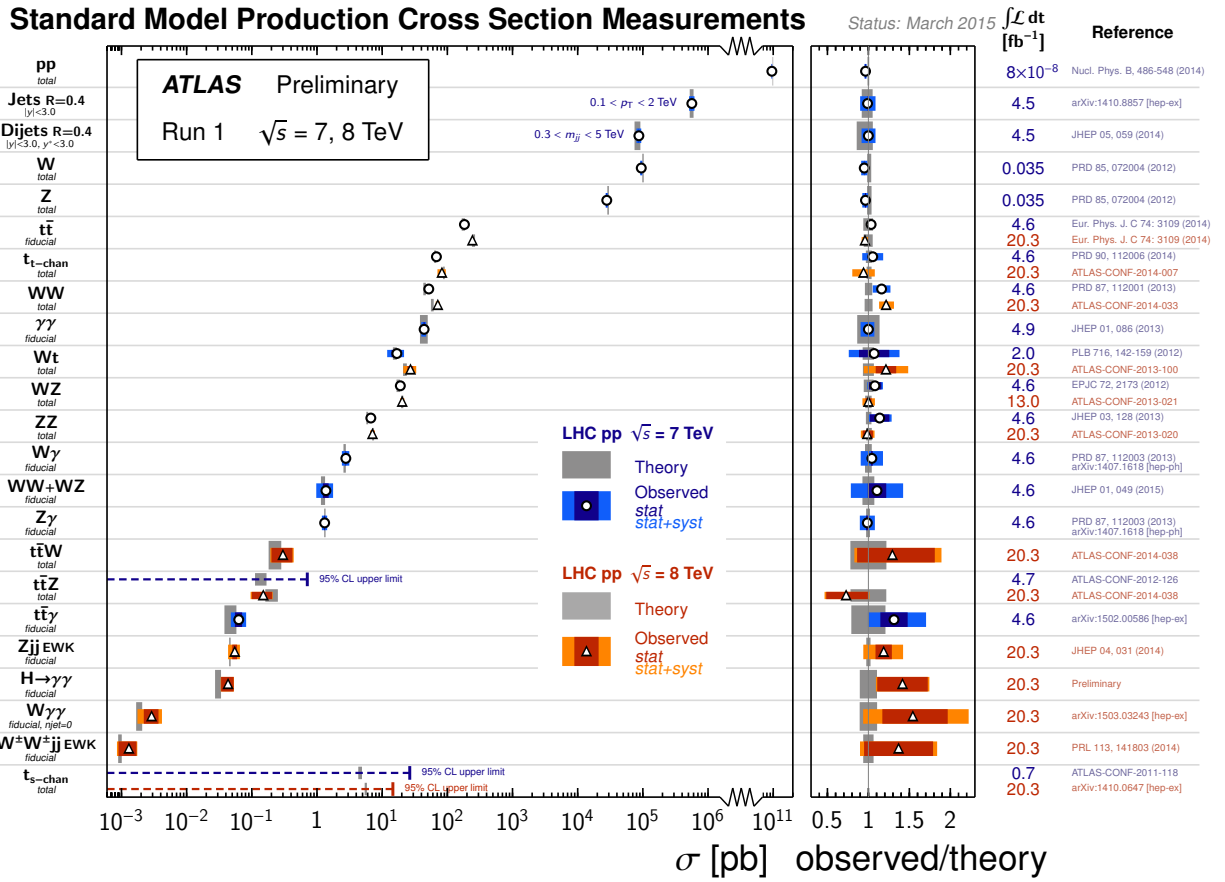


Figure 15: Detailed summary of several Standard Model total and fiducial production cross section measurements, corrected for leptonic branching fractions, compared to the corresponding theoretical expectations [3].

References

- [1] ATLAS Collaboration, *The ATLAS Experiment at the CERN Large Hadron Collider*, JINST **3** (2008) S08003.
- [2] ATLAS Experiment Luminosity Public Results.
twiki.cern.ch/twiki/bin/view/AtlasPublic/LuminosityPublicResults.
- [3] ATLAS Experiment Standard Model Public Results.
twiki.cern.ch/twiki/bin/view/AtlasPublic/StandardModelPublicResults.
- [4] ATLAS Collaboration, *Measurement of the total cross section from elastic scattering in pp collisions at $\sqrt{s} = 7$ TeV with the ATLAS detector*, Nucl. Phys. **B889** (2014) 486–548, arXiv:1408.5778 [hep-ex].

- [5] ATLAS Collaboration, *Measurement of exclusive $\gamma\gamma \rightarrow \ell^+\ell^-$ production in proton-proton collisions at $\sqrt{s} = 7$ TeV with the ATLAS detector*, Phys. Lett. **B749** (2015) 242–261, arXiv:1506.07098 [hep-ex].
- [6] ATLAS Collaboration, *Measurement of distributions sensitive to the underlying event in inclusive Z-boson production in pp collisions at $\sqrt{s} = 7$ TeV with the ATLAS detector*, Eur. Phys. J. **C74** no. 12, (2014) 3195, arXiv:1409.3433 [hep-ex].
- [7] ATLAS Collaboration, *Measurements of the W production cross sections in association with jets with the ATLAS detector*, Eur. Phys. J. **C75** no. 2, (2015) 82, arXiv:1409.8639 [hep-ex].
- [8] ATLAS Collaboration, *Measurement of the low-mass Drell-Yan differential cross section at $\sqrt{s} = 7$ TeV using the ATLAS detector*, JHEP **06** (2014) 112, arXiv:1404.1212 [hep-ex].
- [9] ATLAS Collaboration, *Measurement of the forward-backward asymmetry of electron and muon pair-production in pp collisions at $\sqrt{s} = 7$ TeV with the ATLAS detector*, JHEP **09** (2015) 049, arXiv:1503.03709 [hep-ex].
- [10] ATLAS Collaboration, *Measurement of the WW + WZ cross section and limits on anomalous triple gauge couplings using final states with one lepton, missing transverse momentum, and two jets with the ATLAS detector at $\sqrt{s} = 7$ TeV*, JHEP **01** (2015) 049, arXiv:1410.7238 [hep-ex].
- [11] ATLAS Collaboration, *Evidence of $W\gamma\gamma$ Production in pp Collisions at $\sqrt{s} = 8$ TeV and Limits on Anomalous Quartic Gauge Couplings with the ATLAS Detector*, Phys. Rev. Lett. **115** no. 3, (2015) 031802, arXiv:1503.03243 [hep-ex].
- [12] ATLAS Collaboration, *Evidence for Electroweak Production of $W^\pm W^\pm jj$ in pp Collisions at $\sqrt{s} = 8$ TeV with the ATLAS Detector*, Phys. Rev. Lett. **113** no. 14, (2014) 141803, arXiv:1405.6241 [hep-ex].
- [13] ATLAS Collaboration, *Measurement of the inclusive jet cross-section in proton-proton collisions at $\sqrt{s} = 7$ TeV using 4.5 fb^{-1} of data with the ATLAS detector*, JHEP **02** (2015) 153, [Erratum: JHEP09,141(2015)], arXiv:1410.8857 [hep-ex].
- [14] ATLAS Collaboration, *Measurement of three-jet production cross-sections in pp collisions at 7 TeV centre-of-mass energy using the ATLAS detector*, Eur. Phys. J. **C75** no. 5, (2015) 228, arXiv:1411.1855 [hep-ex].
- [15] ATLAS Collaboration, *Measurement of the inclusive isolated prompt photons cross section in pp collisions at $\sqrt{s} = 7$ TeV with the ATLAS detector using 4.6 fb^{-1}* , Phys. Rev. **D89** no. 5, (2014) 052004, arXiv:1311.1440 [hep-ex].